3D Printing and Growth Induced Bending based on PET-RAFT Polymerization

Chris William Anderson Bainbridge[#], Kyle Edward Engel[#], and Jianyong Jin[*]

[a] *School of Chemical Sciences, The University of Auckland, Auckland 1010, New Zealand*

[b] *Dodd-Walls Centre for Quantum and Photonic Technologies, Auckland 1010, New Zealand*

[#] *Authors contributed equally to the work*

ORCID:

Chris Bainbridge: 0000-0002-6135-3382

Kyle Engel: 0000-0003-3749-6890

Jianyong Jin: 0000-0002-5521-6277

KEYWORDS:

3D printing, 4D printing, PET-RAFT polymerization, post-3D printing modification, trithiocarbonate, growth induced bending

ABSTRACT

4D printing has steadily become an emerging area of advanced manufacturing research and has produced some truly fantastic innovations. Previously we have demonstrated the 3D printing process based on PET-RAFT polymerization, and its subsequent capability in the post-production modification of surface properties. In this work, (1) we further optimized the PET-RAFT 3D printing formulation by replacing RAFT agent CDTPA with BTPA and adjusting the monomers composition; (2) we also observed the photodegradation of the photocatalysts EB and EY under 405nm light and the effects this has on 3D printing; (3) we then did successful 3D printing using a commercial 405nm DLP 3D printer, with an improved build speed of up to 2286 μm/hr; (4) lastly, for the first time we have demonstrated a method for growth induced bending of a 3D printed strip, where the growth on one side of the strip causes stress and the strip bends accordingly to reach a more comfortable position.

GRAPHIC ABSTRACT

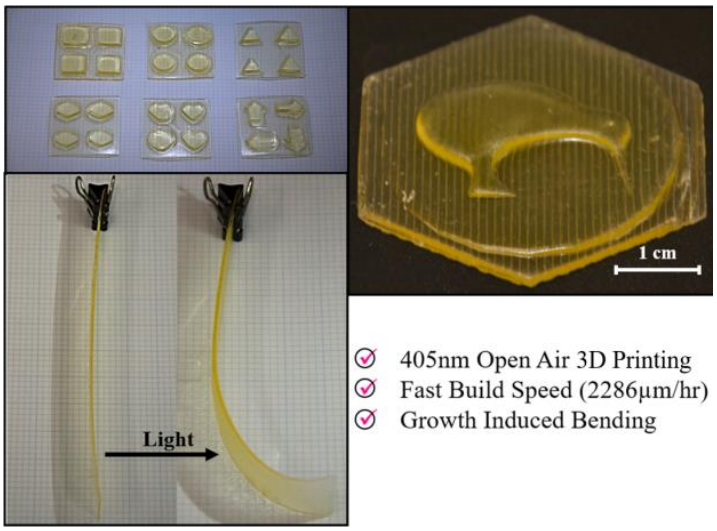

1. INTRODUCTION

The development of 3D printing since the early 1980's has seen this unique production technique become a popular and viable method for the rapid manufacturing of bespoke prototypes, which has had a profound effect on the direction of materials science[1]. 3D printing allows for the production of complex single-run products with a wide range of materials, including both metals and polymers, with a minimum of difficulty and waste. This widespread utility is granted by the array of available techniques such as; fused deposition modeling (FDM) for thermoplastics, selective laser sintering (SLS) for metals, as well as stereolithography (SLA) and digital light processing (DLP) for vat photopolymerization using monomer resins[2, 3]. Recent developments since the expiration of the FDM patents in 2009 have driven the market to develop an array of both large industrial printers, as well as smaller desktop printers for use by regular consumers[4]. Many see these developments as a key part of the 4th industrial revolution, a term used to refer to the synchronous development of smart materials, increasing availability of bespoke manufacturing, and improvements in artificial intelligence[5, 6]. The role of 3D printing for on-demand manufacturing is very clear, but it has been further recognized as having uses in the realm of smart materials through techniques classified as 4D printing[6, 7].

4D printing encompasses the entire range of 3D printable smart materials. The majority of these use responsive materials to react to an environmental stimulus, or to return to their original form after deformation. Recent notable examples in 4D printing include those such as; Ge et al, who created a system which combined independently activated photo and thermal components, using this they were able to produce 3D printed objects with both shape memory properties and high reprocessability[8]. Schwartz and Boydston demonstrated an example of dual wavelength 3D printing by using a resin containing components activated separately by UV (for cationic initiation) and visible (for radical initiation) wavelengths, allowing them to produce objects which could undergo swelling induced actuation due to their multi-material composition[9]. There are many potential options for further 3D/4D printing development, particularly those that provide a platform for which other techniques can then be applied.

One such proposal by Johnson and coworkers for further 3D/4D printing research was to create "living" polymeric materials through the incorporation of reversible deactivation radical polymerization (RDRP) constituents into the final structure, in a process they termed "living additive manufacturing"[10]. Such RDRP techniques are considered "living" due to their ability to continue polymerizing on-demand after their initial usage. This would combine the high versatility of controlled polymerization techniques with the structural complexity of 3D printing, allowing for the manufacturing of structures with significant post-production modularity and functionality[7, 11]. Of all the available 3D printing techniques it was quickly decided that vat photopolymerization and broader photo-chemistry would provide the most suitable approach. Light based 3D printers have several key advantages over other methods; spatiotemporal control both before and after printing, relative lack of harmful conditions, ability to use temperature sensitive compounds, high biocompatibility, and energy/wavelength selectivity[11, 12].

However, this forms only half of the solution, with the next choice being which RDRP technique was most appropriate for the task. In recent years Boyer and Xu at UNSW have put significant effort into the development of photo electron/energy transfer reversible addition-fragmentation chain-transfer (PET-RAFT) polymerization, which in simpler terms is a photo-catalyzed mechanism for RAFT polymerization[13-15]. Since their initial development in 1998, RAFT processes have shown remarkable versatility as a controlled polymerization technique[16, 17], with notable uses in block copolymerization and self-assembling macromolecules[18, 19]. When it comes to polymerization in network structures, there is the choice between symmetric and asymmetric RAFT agents. Within a network a symmetric RAFT agent will provide intra-network growth in size and mass by expanding the chains between crosslinking points, whereas an asymmetric RAFT agent will also cause network-wide growth but only at the chain ends, making it more suitable for surface growth and functionalization[20]. Previously our group has demonstrated 3D printing techniques based on photo-RAFT polymerization under various visible wavelengths (405nm, 483nm and 532nm) ; both via an iniferter mechanism under an inert atmosphere[21], and via PET-RAFT in open air[22]. In both studies we demonstrated the facile surface modification that could be performed on the samples after printing with a range of different monomers; pyrene methyl methacrylate (PyMA) for a light response, N-isopropylacrylamide (NIPAM) for temperature response, and butyl acrylate (BA) to modify the surface hydrophobicity.

For this work, we further optimized the PET-RAFT 3D printing formulation and demonstrated the 3D printability using a commercial DLP 3D printer with standard 405nm light sources. We also explore the 4D post-production modification capabilities of the 3D printed object using green light (λ_{max} = 532 nm). To do so we demonstrate spatially controlled directional movement of 3D printed strips in the form of curling and bending. The use of light activation allows such post-production modification to be easily controlled both spatially and temporally under mild conditions, providing a new dimension to 4D “living” polymer materials.

2. RESULTS AND DISCUSSIONS

2.1. 3D-RAFT Printing Resin Formulation and Properties

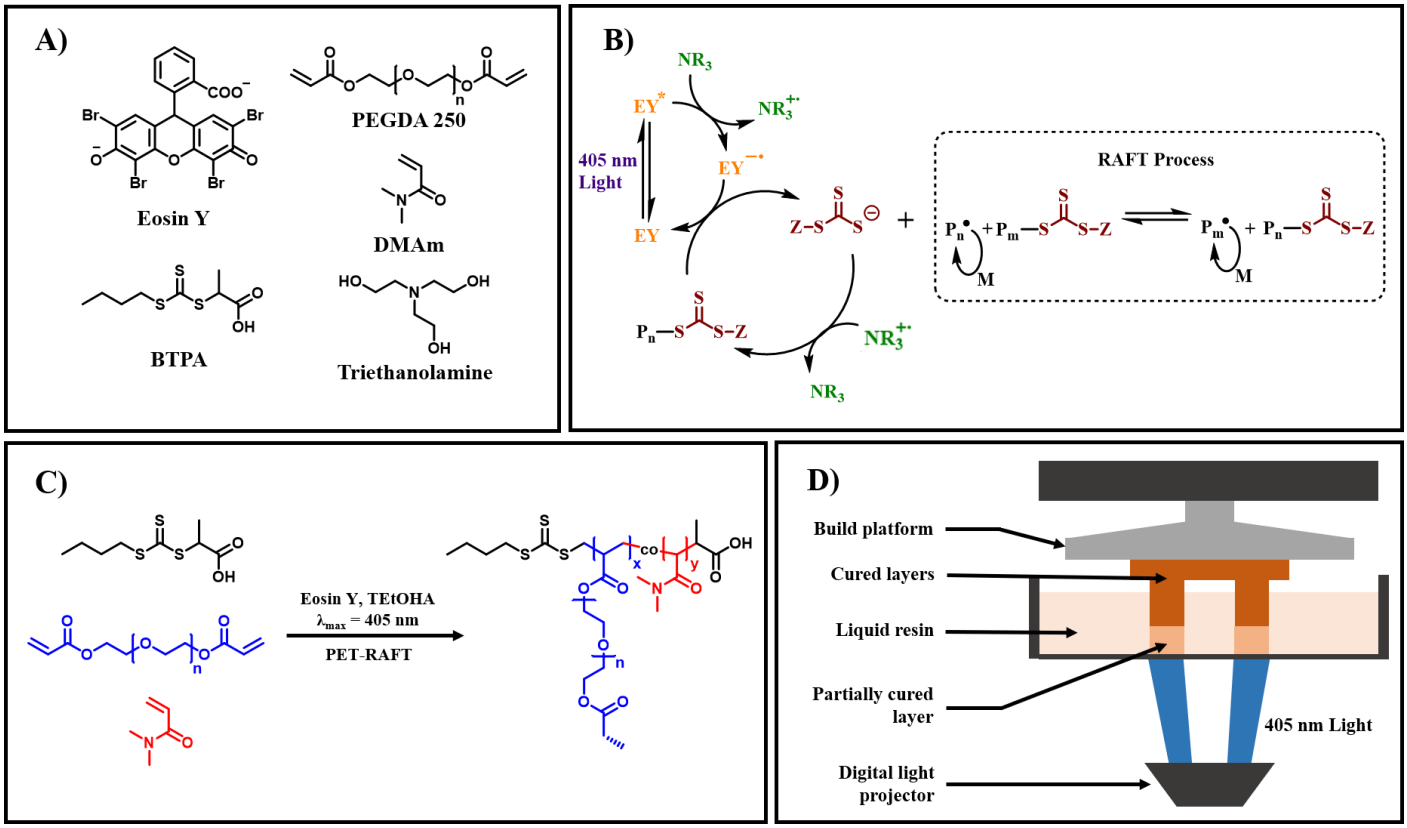

Figure 1. (A) Chemical structures of Eosin Y (EY), 2-(butylthiocarbonothioylthio) propanoic acid (BTPA), poly (ethylene glycol) diacrylate (PEGDA, average M_n = 250 g/mol), N, N-dimethylacrylamide (DMAm), and triethanolamine (TEtOHA). (B) Proposed combined photo electron/energy transfer (PET) RAFT mechanism showing the tertiary amine pathway by Qiao, Boyer, and Nomeir[15, 23-25] (C) Reaction scheme for the PET-RAFT polymerization of our 3D printing resin. (D) Schematic for the working diagram of a standard DLP projector 3D printer.

Our group has previously worked on RAFT based 3D printing using both iniferter[21] and PET-RAFT[22] processes. Our collaborator the Boyer group have also shown good work with an aqueous based RAFT 3D/4D printing system[15]. The basic recipe for iniferter photo-RAFT 3D printing contains only acrylate monomers to be polymerized and RAFT agent, which is directly activated by the light source. The PET-RAFT recipe contains these same basic components with the addition of a photo redox catalyst and a tertiary amine, as seen in Figure 1A. In this process the photocatalyst such as Eosin Y (EY) is raised to an excited state (EY*) under irradiation where it then has several pathways to release its energy[25]. The excited EY* can transfer energy to the natural triplet oxygen, or it can transfer energy/electron to the RAFT agent to initiate PET-RAFT polymerization[23]. The inclusion of a tertiary amine provides an additional pathway shown in Figure 1B, where the tertiary amine acts as an electron donor to reduce the EY* to the EY radical anion ($EY^{-\bullet}$), which must then reduce the polymeric RAFT agent ($S=C(Z)S-P_n$).[25]. This tertiary amine pathway is particularly useful, as it is an oxygen tolerant pathway which is highly desirable and necessary for any 3D printing system[15, 22].

In our prior PET-RAFT 3D printing work we used a 3D printing resin composed of [CDTPA]: [PEGDA]: [EY]: [TEA], which was able to be printed under both blue (λ_{max} = 483 nm, 4.16 mW/cm^2) and green (λ_{max} =

532 nm, 0.48 mW/cm^2) lights[22]. This resin was slower to polymerize compared to conventional free radical polymerization (FRP) equivalents and produced objects with a maximum build speed of 1354 µm/hr under green light. Furthermore, these printed objects were brittle due to 100% of bifunctional PEGDA content. Therefore, within this work we opted to make several changes to the resin as remedies to the problems outlined here.

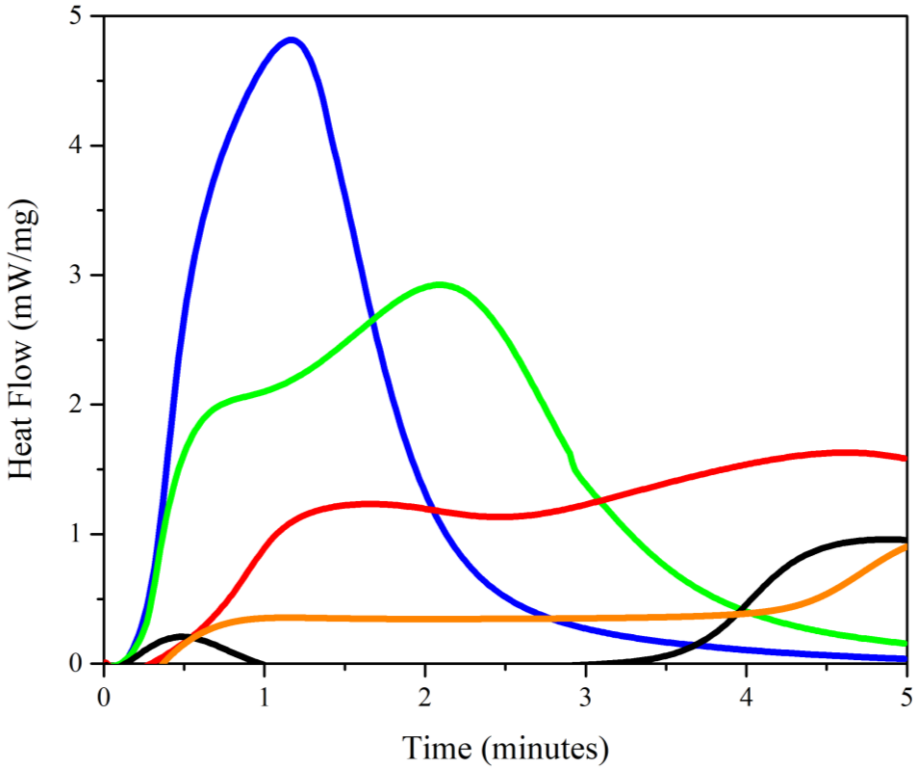

Figure 2. Photo-DSC plot showing resin composition of [BTPA]: [PEGDA]: [EY]: [TEtOHA] = 1:500:0.01:20 (**blue** trace), [BTPA]: [PEGDA]: [DMAm]: [EY]: [TEtOHA] = 1:350:150:0.01:20 (**green** trace), [BTPA]: [PEGDA]: [DMAm]: [EY]: [TEtOHA] = 1:150:350:0.01:20 (**red** trace), [CDTPA]: [PEGDA]: [EY]: [TEOHA] = 1:500:0.01:20 (**black** trace) and [CDTPA]:[PEGDA]:[EY]:[TEA] = 1:200:0.01:2 (**orange** trace) form our previous PET-RAFT work[22], were compared to find an optimum new resin formula. The effects of different RAFT agent and comonomer ratio are noticeable on both the maximum heat flow and the peak position of t_{max}.

The development of an optimized 3D printing resin formula for use in a commercial DLP printer (λ_{max} = 405 nm, 101.86µW/cm^2) was the first step in this research. Thus, several criteria were used to determine the quality of the optimized resin; the optimized resin must be able to hold its form in 60 seconds or less exposure time, the printed objects must have a good layer to layer resolution and binding, must be an accurate representation of the CAD model, and the resin must be stable enough to be reusable for consecutive runs.

With these criteria as a guide, several new resin recipes were formulated and tested using Photo Differential Scanning Calorimetry (Photo-DSC) with a light source range of 400-500nm. A monomer to RAFT agent ratio of 500:1 was chosen as a balance between a faster build speed, and a high enough RAFT concentration to perform post-production modifications. For the first step in optimization we decided to compare two

asymmetric RAFT agents, CDTPA and BTPA. We used photo-DSC to determine their relative speeds, by monitoring both their rate of polymerization and inhibition period. As shown in Figure 2, the resin formula of [BTPA]: [PEGDA]: [EY]: [TEtOHA] = 1:500:0.01:20 (**blue** trace) shows a very limited inhibition period. Additionally, the **blue** trace displays a much earlier t_{max} (an indication of the time to reach maximum reaction rate and hence network formation) at 1.2 minutes and a heat flow of 4.8 mW/mg. When replacing BTPA with CDTA and keeping other parameters intact, the **black** trace, [CDTPA]: [PEGDA]: [EY]: [TEtOHA] = 1:500:0.01:20, showed a much longer inhibition period with a t_{max} that does not occur within 5 minutes. These results help to demonstrate the increase in polymerization rate that can be achieved by using BTPA in place of CDTPA. Furthermore, comparing the **blue** trace to our previous PET-RAFT resin (**orange** trace) ([CDTPA]: [PEGDA]: [EY]: [TEA] = 1:200:0.01:2)[22] this new resin that makes use of BTPA still showed a significantly earlier t_{max}, compared to about 8 minutes for our previous resin[22].

The use of DMAm as a comonomer was explored in ratios of [PEGDA]: [DMAm] = 70:30 and 30:70. DMAm was included due to its high glass transition temperature (T_g) (~90°C)[26], compared to the T_g of PEGDA which is below 0˚C[27], thus helping to reduce the crosslink density and make the network tougher. For the resin formula [BTPA]: [PEGDA]: [DMAm]: [EY]: [TEtOHA] = 1:350:150:0.01:20 (**green** trace), the addition of DMAm slowed down the polymerization rate with the t_{max} being shifted to 2.1 minutes, as seen in Figure 2. With a higher ratio of DMAm in the resin the **red** trace ([BTPA]: [PEGDA]: [DMAm]: [EY]: [TEtOHA] = 1:150:350:0.01:20) showed an even slower polymerization rate with the t_{max} now shifted to 4.6 minutes. However, even with these decreases in t_{max} both traces still showed a limited inhibition period and faster polymerization rate compared to the CDTPA based formulation (**black** trace and **orange** trace).

As seen in Figure 2, these comonomer resins (**green** and **red** trace) displayed a bimodal peak distribution. The first peak in these traces could be attributed to the conventional linear copolymerization of PEGDA and DMAm, while the second peak may be assigned to the energy released during the crosslinking process at the point of gelation. Hence, the second peak in the **green** trace being sharper and earlier than in the **red** trace, due to the crosslinking ratio in the **green** trace being much higher ([PEGDA]: [DMAm] = 70: 30 versus 30: 70).

While the inclusion of DMAm does appear to negatively influence the heat flow curves of the resin, however, the DSC data alone would not be solely representative in determining the most optimal resin in actual 3D printing process. After exploring the print resolution and build speeds for resins of [PEGDA]:[DMAm] ratios 100:0, 70:30 and 30:70 in the commercial DLP printer, the monomer molar ratio [PEGDA]:[DMAm] = 70:30 showed the best results when considered against the criteria outlined earlier and was noticeably less brittle than our previously 3D printed pure PEGDA objects[22]. This ratio produced the most resolved objects with a normal layer exposure time of 30 seconds and a thickness of 30µm for each layer. This yields a 3600 µm/hr theoretical build speed ((30 µm layers / 0.5 minutes) × 60 minutes, movement of the build platform excluded). Compared to the max build speed of previous work by our group, 1354 µm/hr[22], this theoretical build speed

was promising. This resin formulation was later used to print all samples for both dynamic mechanical analysis (DMA) and 4D post-production modification.

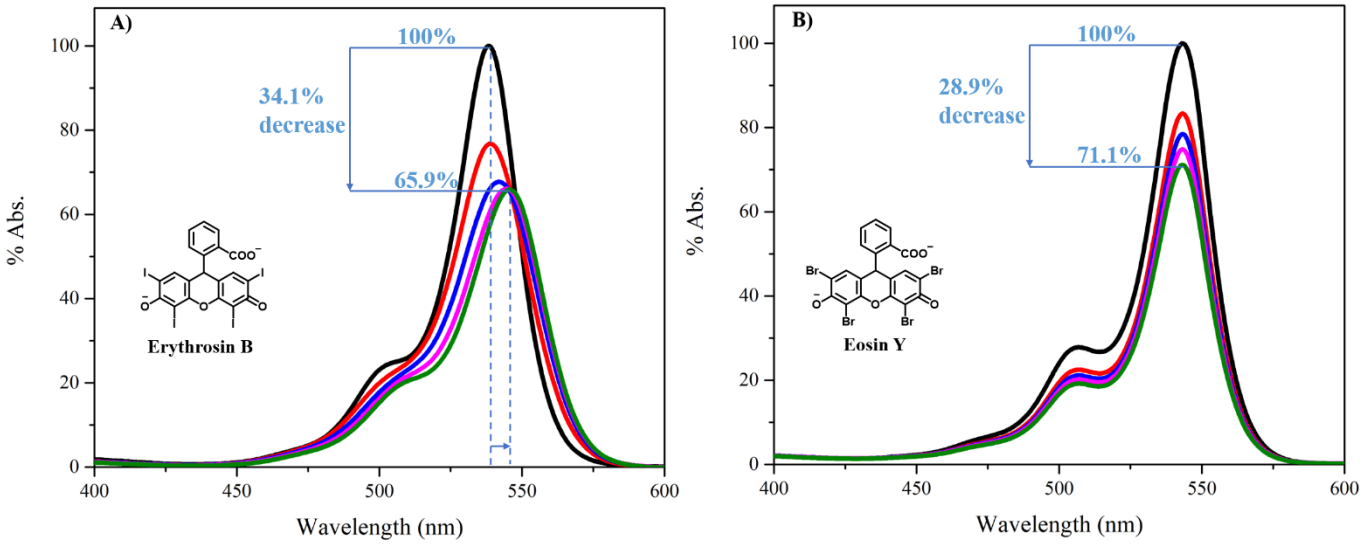

Figure 3. UV-Vis absorption spectra; (A) EB under 405nm (397.45μW/cm^2) exposure for; initial (**black** trace), 10 minutes (**red** trace), 20 minutes (**blue** trace), 30 minutes (**magenta** trace) and 40 minutes (**olive** trace). (B) EY under 405nm exposure for; initial, 10 minutes, 20 minutes, 30 minutes and 40 minutes.

As mentioned previously our group is aware of the issues with using 405nm light sources for PET-RAFT processes, not only the possibility of the competing iniferter process, but also the possibility of degradation of organic dyes[14, 28] despite the poor absorbance of these catalysts in the near UV region. It is important and ideal for any photocatalytic process that the photocatalyst does not display symptoms such as photodegradation[14, 29] or photobleaching[30, 31] over the course of its use. Figure 3 shows the comparison between two common organic photocatalysts, Eosin Y (EY) and Erythrosin B (EB), using their absorbance curves after different periods of 405 nm light irradiation (397.45μW/cm^2). Both showed a noticeable gradual decrease in UV absorbance which could likely be due to irreversible photodegradation, given that the effect remains after the sample has been stored overnight in a dark environment and measured again. The absorbance loss over time can be clearly seen in Figure 3A where EB showed drops to 76.8%, 67.7%, 66.0%, and 65.9% of the initial absorbance, after 10, 20, 30, and 40 minutes respectively at each of its peak maxima. While in Figure 3B, EY showed drops to 83.3%, 78.4%, 74.8%, and 71.1% of the initial absorbance, over the same period and intervals. This was complicated by the EB absorbance peak which showed a significant redshift as they decrease (shifting from 538 nm to 546 nm, after 40 minutes irradiation time); however, the pattern of lower corresponding values to EY was retained at 543 nm. After periods of 40 minutes and longer the EB solution began to visibly change color from a bright pink-red to a more faded hue, but this observation did not carry over to the EY samples, which even after 1.5 hours of 405 nm irradiation showed no visible loss of color. Because of these results we opted to retain EY in our 3D-RAFT resin composition, as it is important to have

a relatively photostable catalyst to allow the printing process to go undisturbed for the full length of the printing duration. Under our printing parameters, notably wavelength and light intensity, the objects were limited to a total print time of about 1 hour. After this length of time the print showed noticeable differences from the CAD model which would render it unsuccessful. To avoid these issues in future work, we must find a more suitable photocatalyst for this wavelength.

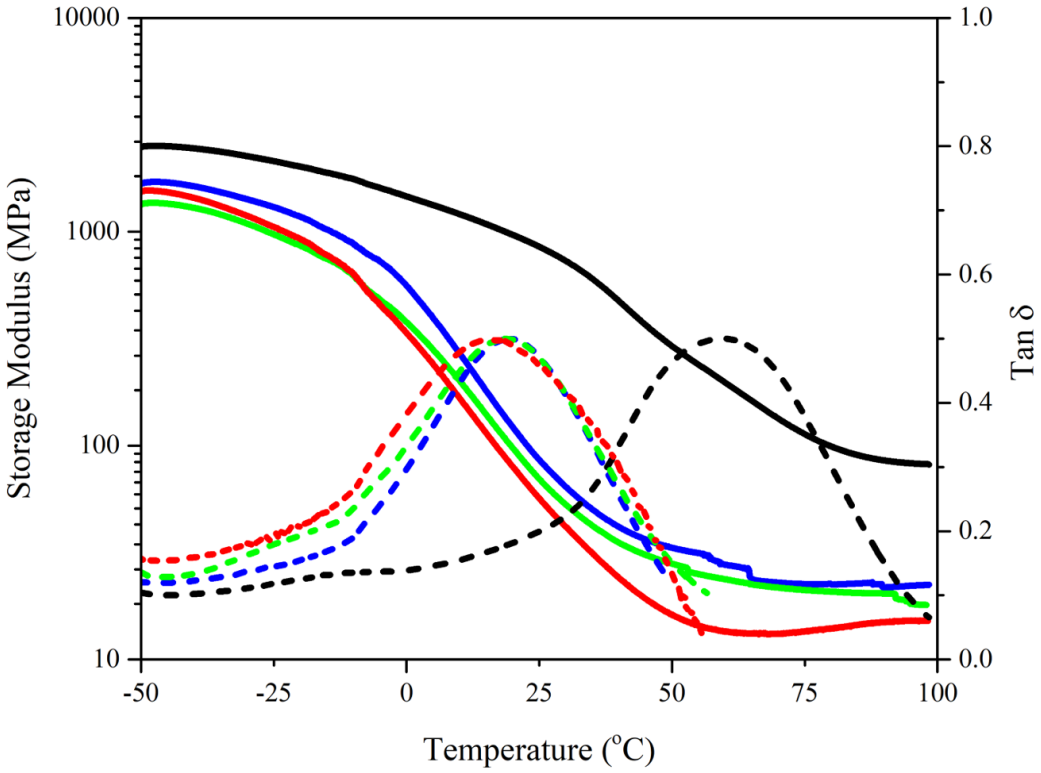

Figure 4. DMA plot showing; (**black** trace) the storage modulus (E') and (**black** dashed trace) Tan δ from the 3D printed DMA rectangular sample by normal FRP of resin formula [PEGDA]: [DMAm]: [TPO] = 350:150 and 2wt% TPO; (**blue** trace) the E' and (**blue** dashed trace) Tan δ from 3D-RAFT printed DMA sample using resin formula [BTPA] :[PEGDA]: [DMAm]: [EY]: [TEtOHA] = 1:350:150:0.01:20; (**green** trace) the E' and (**green** dashed trace) Tan δ from the post-printing modified DMA sample; lastly (**red** trace) the E' and (**red** dashed trace) Tan δ from the non-3D printed DMA sample prepared by normal PET-RAFT polymerization in bulk. Duplicate measurements were performed to ensure the validity of the reported results.

DMA analysis was performed on four different rectangular samples with dimensions 40 × 12 × 1.6 mm (length × width × thickness). These were; samples 3D printed using the optimized RAFT resin both before and after post-production modification, a non-3D printing DMA sample by PET-RAFT polymerization in bulk and a 3D printed free radical polymerization (FRP) control sample. For each batch, six 3D-RAFT resin DMA samples were printed simultaneously on one build platform using a layer thickness of 30 µm an attachment

time of 60 seconds and a normal exposure time of 30 seconds per layer (53 layers total). While the non-3D printed RAFT sample was produced using the same optimized formula but polymerized in bulk using an external mold and a conventional 405nm lamp external (397.45μW/cm^2) (see the Supporting Information for details). FRP samples were printed using the same 3D printing parameters and monomer composition but used a common conventional photoinitiator, phenylbis (2, 4, 6-trimethylbenzoyl) phosphine oxide (TPO) (see the Supporting Information for details).

To determine the storage modulus (E') and glass transition temperature (T_g) of the 3D printed objects, a temperature ramp (2˚C/min) was performed with a constant displacement frequency (1Hz). The objects were held at -50˚C for 5 minutes before heating to 100˚C. E' was calculated at room temperature (20˚C) and T_g was determined from the peak of the Tan δ curve. As shown in Figure 4 **blue** trace the sample printed with 3D-RAFT resin had an E' in the range of 140 MPa at room temperature and a T_g of about 19˚C. When compared to results obtained by the Boyer group[15], also making use of the same monomer ratio of [PEGDA]: [DMAm] = 70:30, they reported an E' of 250 MPa and a T_g of 30˚C. Some differences were expected given that the Boyer group utilized Erythrosin B (EB) as their organic photocatalyst and performed their 3D printing using green light with a layer thickness of 20μm (80 layers total).

When compared to non-3D printed bulk samples polymerized in a mold using the same conditions (see the Supporting Information for details), there was a significant change in the E' to 80 MPa and T_g to 15˚C (Figure 4 **red** trace). Given there are significant differences in the manufacturing process of the DLP 3D printer compared to a molding process, we expected to see different DMA results from these samples. This layer-by-layer construction appeared to play a major role in the E' at room temperature of the overall sample (Figure 4 **blue** vs **red** traces). Each layer in the 3D printed sample received equal light irradiation (apart from attachment layer where specified), whereas in the bulk samples light had to penetrate through the entire thickness of the resin.

For the 3D printed FRP sample of resin composition [PEGDA]: [DMAm]: [TPO] = 350:150 and 2wt% TPO, the E' value was much higher at around 1300 MPa with a T_g of about 58˚C (Figure 4 **black** trace). This difference in E' and T_g can be attributed to the presence of the RAFT agent BTPA lowering the degree of crosslinking and generating a higher number of chains ends in the RAFT mediated sample. This has been described by Flory and others, that as a result of these factors the networks have a higher free volume, and thus a lower E' and T_g [32-34].

The post-production modification of objects printed using 3D-RAFT printed objects is explored in greater detail in section 2.2 of this article. However, the effect of post-production modification on the mechanical properties and the relative effect on E' and T_g of the sample can be analyzed using DMA. Rectangular samples 3D printed using RAFT resin were subsequently modified via methyl methacrylate (MMA) monomer insertion performed in a growth medium devoid of solvent (see the Supporting Information for details). The E' at room temperature of the sample had decreased to 100 MPa but the T_g remained constant at about 19˚C (Figure 4

green trace). These limited changes can largely be attributed to the fact that BTPA is an asymmetric RAFT agent, all the growth being surface focused thus limiting the mechanical effects on the 3D printed RAFT sample. This will be discussed further in section 2.2 at molecular level.

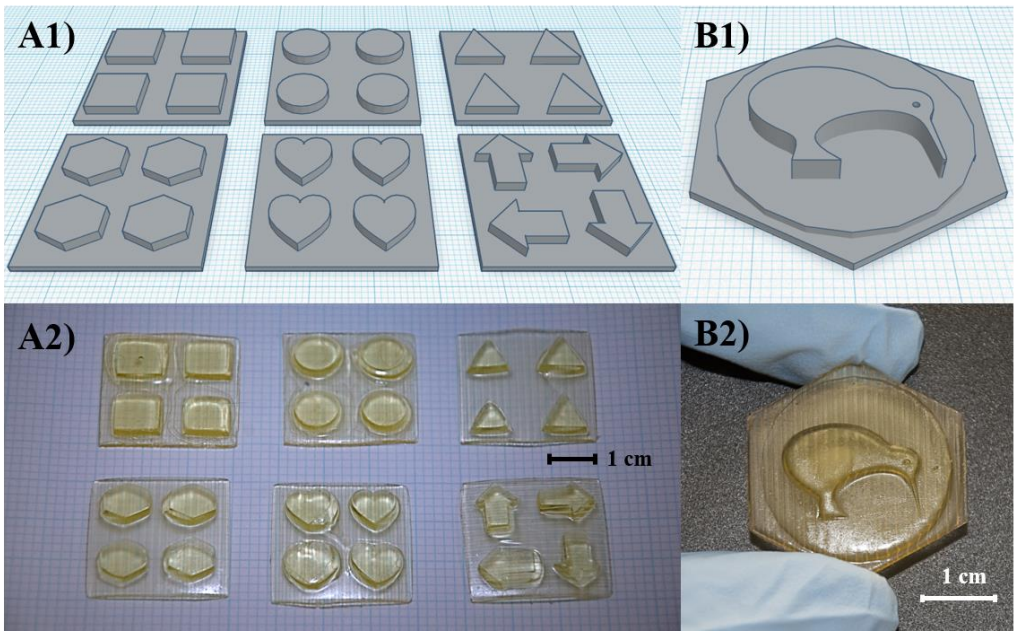

Figure 5. Optical images and corresponding CAD models for the 3D-RAFT printed objects. A1) CAD model for shapes upon 3 × 3 cm base. A2) Corresponding 3D-RAFT objects printed using the DLP 3D printer. B1) Kiwi bird CAD model upon tiered base. B2) Corresponding 3D-RAFT printed object.

With our RAFT 3D printing resin prepared, we embarked on designing the CAD models for the desired objects, as well as setting the relevant parameters. Each layer was programmed to a uniform thickness of 30µm with an exposure of 30 seconds. While in order to ensure proper attachment to the build platform, we used an initial attachment time of 60 seconds for the first 15 layers.

As shown in Figure 5 various shapes were arranged on square base plates to observe how well the new PET-RAFT resin formula handled different features, such as curves and corners. These objects generally represented an accurate 3D print of the corresponding CAD model, confirming that the current 3D-RAFT resin was capable of printing 3D objects using a 405nm DLP 3D printer (λ_{max} = 405 nm, 101.86µW/cm^2). To demonstrate this fact further we printed another model with a kiwi on a circular coin, and a hexagonal base plate, the print of which was very similar to the original model. Objects printed with 3D-RAFT also displayed an actual build speed of 2286 µm/hr (calculated from the actual height of printed objects over the full print time) consistent with that of the theoretical build speed, which is significantly faster than our previous PET-RAFT resin formula ([CDTPA]: [PEGDA]: [EY]: [TEA] = 1:200:0.04:3) at 1354 µm/hr [22]. Objects printed with the 3D-RAFT resin also showed very limited shrinkage after printing, keeping their intended thickness to within ±0.5 mm error. 3D-RAFT printed objects were washed in ethanol, THF, and DMSO for 2 days in each solvent, and there was no visible loss in the yellow color arising from the trithiocarbonate group of the

RAFT agent. Additionally, this 3D-RAFT resin showed good robustness and reusability over more than 10 separate prints and after being stored in a refrigerator for 3 weeks without light exposure.

Having demonstrated that we could reliably print objects using our new RAFT resin, we endeavoured to demonstrate that these objects had retained their desired "living" behavior and could undergo post-production modification. Previously our group has shown the facile post-production surface modification of 3D-RAFT printed objects. In this work, to further demonstrate this aspect of the RAFT agent containing polymer networks' capabilities we decided to show how the spatially controlled insertion of monomer could be used to induce bending behaviour in 3D-RAFT printed strips.

2.2. Growth Induced Bending

The ability to induce movement or actuation in an object is one of the more popular examples of 4D modification for a multitude of reasons. 4D movement allows for the creation of highly customizable devices such as; medical implants which move and grow within the body[35-37], sensors which move upon stimulation[38, 39], and various soft robotics applications[40, 41]. There are many different pathways to achieving such movement in 3D printed objects, common examples include; solvent swelling and expansion[42-45], thermally induced contraction[46-50], pneumatic force through printed channels[38, 41, 51], photochemical changes (cis-trans isomerization, reversible ring opening, cycloaddition, and bond-exchange)[52-54], and spatioselective printing of areas of high and low stress[55, 56]. Of all these techniques, the least explored is the use of non-uniform stress to induce movement to a more "comfortable" position. The best example of this stress induced bending being the "photo-origami" of Ryu et al, where UV light was used to rearrange the crosslinking of the network thus inducing curvature from the stress gradient[56].

In our work, a 3D-RAFT printed strip was printed using the following specifications; 120 × 20 × 0.6 mm (length × width × thickness), 20 layers of 30μm thickness each. The sample was homogeneous in nature as each layer was given 60 seconds of exposure in the DLP 3D printer (λ max = 405 nm, 101.86 μW/cm^2) (Figure 6A). Half of this strip was then immersed in a growth medium containing; [BA]: [EY]: [TEtOHA] = 500:0.01:20 in DMSO, and a green LED light (532nm, 58.72 μW/cm^2) was uniformly directed onto one face of the strip (see the Supporting Information for details). As seen in Figure 6B, after 15-minute exposure, the strip showed moderate curvature. Upon further exposure until a total of 30 minutes (Figure 6C) significant bending was observed, and the strip took on a shape akin to that of a hockey stick. After this length of exposure the strip was noticeably softer, and the irradiated face was also paler than the opposite face. The growth medium was also cloudier and turbid after 30 minutes of irradiation. After further irradiation there was little to no change in the curvature of strip, but this was likely due to the angle of light. The strip was initially set up perpendicular to the irradiation direction, but after 30 minutes a significant portion of the strip had bent almost parallel, heavily limiting the irradiated area and thus cease bending. While this study was demonstrative rather than quantitative, the rate of curling appears to be on a similar time scale to other photo-bending techniques available[56, 57].

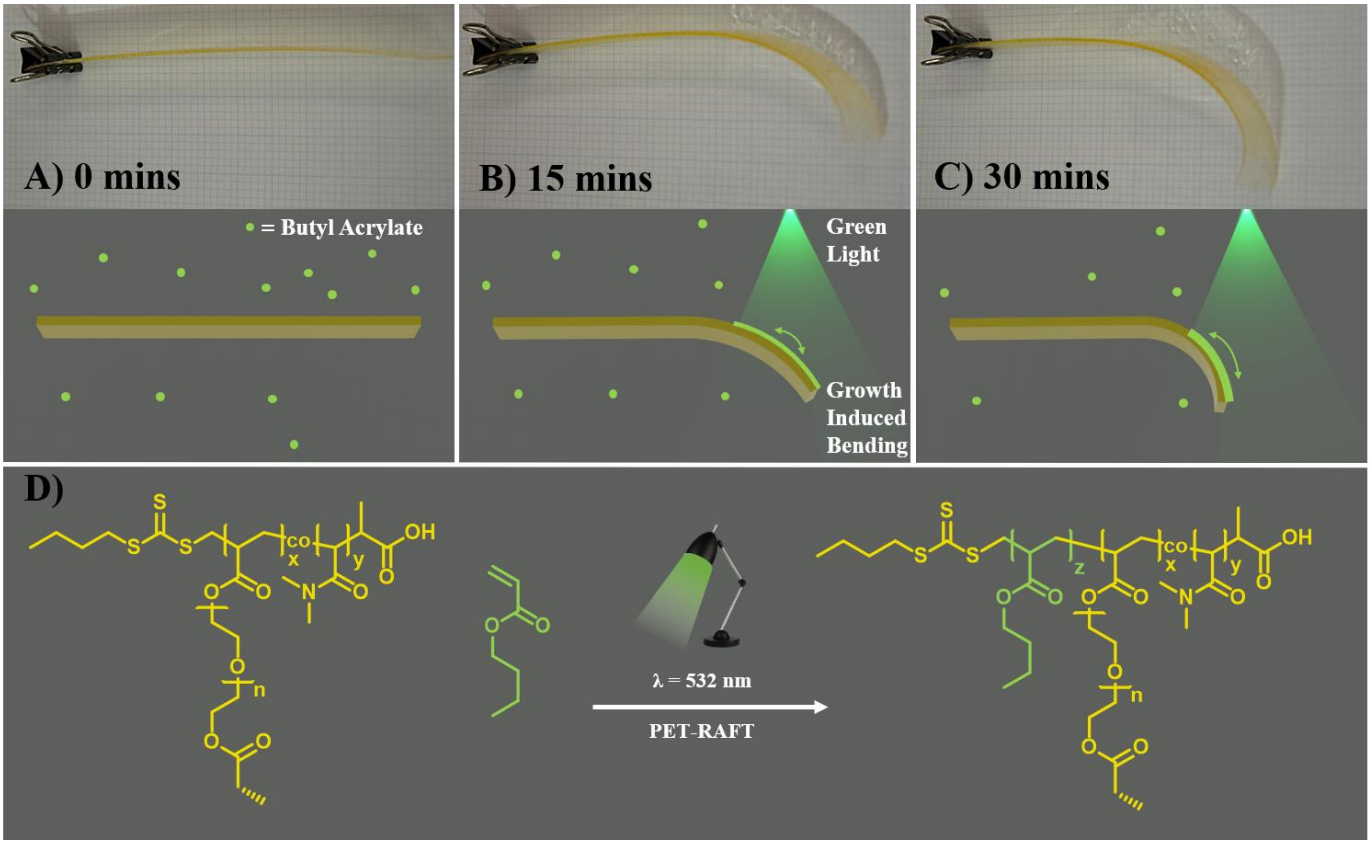

Figure 6. Optical images (top) and graphical representations (bottom) of the growth induced bending process. (A) The initial 3D-RAFT printed strip. (B) The 3D-RAFT strip after 15 minutes monodirectional green light irradiation (532nm, 58.72μW/cm^2) in a growth medium of DMSO and BA. (C) The same 3D-RAFT strip after 30 minutes monodirectional green light irradiation in the same growth medium. (D) Reaction scheme for the photo-catalyzed insertion of BA monomer under green light irradiation (532nm, 58.72μW/cm^2).

To the best of our knowledge, this is the first demonstration of the growth of new material into the surface of an existing 3D printed object using RAFT polymerization to induce a bending response (Figure 6D). We hypothesized that monomer insertion on one face of a homogeneous 3D-RAFT strip would induce a degree of extra stress in that portion of the polymer network, without significant increase in size and mass, and subsequently induce directionally controlled bending. This growth would occur at the chain end of the existing network, due to the use of an asymmetric RAFT agent (BTPA). While some of these short chains would grow on the surface and outwards, they play very little part in the bending. Instead it is the significant amount of growth which occurs in the sub-surface region that, through increasing the polymer network density on one side of the strip, is the primary cause of non-uniform stress and thus the source of the bending. Given previous studies on surface-initiated PET-RAFT we expect the chain growths to be a maximum of 100 nm[58], but due to the constraints of growth within a network they are likely shorter. This data surrounding the growth induced bending is preliminary and will continue to be studied further on a fundamental level.

In order to confirm that the bending was due to our hypothesized process, we performed several control experiments. The first was to perform the same process with an FRP printed strip; [PEGDA]: [DMAm] =

350:150 and 2wt% TPO, which showed no bending after 30 minutes. Next, we left a 3D-RAFT printed strip soaking in the growth medium for 24 hours without any light irradiation to ensure that the bending was coming from growth rather than an alternate stimulus such as solvent swelling, and no changes were observed. Lastly, we took the bent 3D-RAFT strip and attempted to use the same process to return it to its original straight form by shining the green light from the opposite direction. While largely successful, this process required 3 hours of green light irradiation to bring the bent strip close to its original straight form. This indicates the unfavorability of introducing stress on the opposing side of the strip by our current methods.

3. CONCLUSION

In summary, we have further developed a 3D printable RAFT resin formula with an improved build speed up to 2286 μm/hr and demonstrated its ability to undergo 4D post-production transformation. We first demonstrated a facile method for growth induced bending of 3D-RAFT printed strips which opens an alternative pathway for movement and modification of these printed objects. This work serves as a showcase of the current and future potential of 3D-RAFT in the fields of both living polymer networks and 3D/4D printing.

ASSOCIATED CONTENT

Supporting Information

The following files are available in the Supporting Information: Chemicals, characterizations, and experimental procedures.

AUTHOR INFORMATION

Corresponding Author

Jianyong Jin: j.jin@auckland.ac.nz

Conflicts of interest

The authors declare no competing financial interest.

Acknowledgement

J.J., C.B., and K.E. would like to thank the New Zealand Ministry of Business, Innovation and Employment (MBIE) Endeavour Fund for funding the Advanced Laser Microfabrication for NZ Industries research programme (UOAX-1701). We would also like to thank the University of Auckland for its part in advising

public policy regarding COVID-19, and the healthcare workers who have worked tirelessly during this pandemic.

REFERENCES

1. Hartings, M. R.; Ahmed, Z., Chemistry from 3D printed objects. *Nature Reviews Chemistry* **2019,** *3* (5), 305-314.

2. Griffey, J., The types of 3-D printing. *Library Technology Reports* **2014,** *50* (5), 8-12.

3. Jasveer, S.; Jianbin, X., Comparison of different types of 3D printing technologies. *International Journal of Scientific and Research Publications (IJSRP)* **2018,** *8* (4), 1-9.

4. Cotteleer, M.; Joyce, J., 3D opportunity: Additive manufacturing paths to performance, innovation, and growth. *Deloitte Review* **2014,** *14*, 5-19.

5. Lasi, H.; Fettke, P.; Kemper, H.-G.; Feld, T.; Hoffmann, M., Industry 4.0. *Business & information systems engineering* **2014,** *6* (4), 239-242.

6. Momeni, F.; Liu, X.; Ni, J., A review of 4D printing. *Materials & design* **2017,** *122*, 42-79.

7. Aguilar, M. R.; San Román, J., Introduction to smart polymers and their applications. In *Smart polymers and their applications*, Elsevier: 2019; pp 1-11.

8. Ge, Q.; Sakhaei, A. H.; Lee, H.; Dunn, C. K.; Fang, N. X.; Dunn, M. L., Multimaterial 4D Printing with Tailorable Shape Memory Polymers. *Scientific Reports* **2016,** *6* (1), 31110.

9. Schwartz, J. J.; Boydston, A. J., Multimaterial actinic spatial control 3D and 4D printing. *Nature communications* **2019,** *10* (1), 1-10.

10. Chen, M.; Gu, Y.; Singh, A.; Zhong, M.; Jordan, A. M.; Biswas, S.; Korley, L. T. J.; Balazs, A. C.; Johnson, J. A., Living Additive Manufacturing: Transformation of Parent Gels into Diversely Functionalized Daughter Gels Made Possible by Visible Light Photoredox Catalysis. *ACS Central Science* **2017,** *3* (2), 124-134.

11. Bagheri, A.; Jin, J. Y., Photopolymerization in 3D Printing. *Acs Applied Polymer Materials* **2019,** *1* (4), 593-611.

12. Barner-Kowollik, C.; Bastmeyer, M.; Blasco, E.; Delaittre, G.; Müller, P.; Richter, B.; Wegener, M., 3D laser micro-and nanoprinting: challenges for chemistry. *Angewandte Chemie International Edition* **2017,** *56* (50), 15828-15845.

13. Shanmugam, S.; Xu, J.; Boyer, C., Exploiting metalloporphyrins for selective living radical polymerization tunable over visible wavelengths. *Journal of the American Chemical Society* **2015,** *137* (28), 9174-9185.

14. Xu, J.; Shanmugam, S.; Duong, H. T.; Boyer, C., Organo-photocatalysts for photoinduced electron transfer-reversible addition–fragmentation chain transfer (PET-RAFT) polymerization. *Polymer Chemistry* **2015,** *6* (31), 5615-5624.

15. Zhang, Z.; Corrigan, N.; Bagheri, A.; Jin, J.; Boyer, C., A Versatile 3D and 4D Printing System through Photocontrolled RAFT Polymerization. *Angewandte Chemie* **2019,** *131* (50), 18122-18131.

16. Chong, Y. K.; Le, T. P. T.; Moad, G.; Rizzardo, E.; Thang, S. H., A more versatile route to block copolymers and other polymers of complex architecture by living radical polymerization: the RAFT process. *Macromolecules* **1999,** *32* (6), 2071-2074.

17. Mayadunne, R. T. A.; Rizzardo, E.; Chiefari, J.; Chong, Y. K.; Moad, G.; Thang, S. H., Living radical polymerization with reversible addition− fragmentation chain transfer (RAFT polymerization) using dithiocarbamates as chain transfer agents. *Macromolecules* **1999,** *32* (21), 6977-6980.

18. Derry, M. J.; Fielding, L. A.; Armes, S. P., Polymerization-induced self-assembly of block copolymer nanoparticles via RAFT non-aqueous dispersion polymerization. *Progress in Polymer Science* **2016,** *52*, 1-18.

19. Canning, S. L.; Smith, G. N.; Armes, S. P., A critical appraisal of RAFT-mediated polymerization-induced self-assembly. *Macromolecules* **2016,** *49* (6), 1985-2001.

20. Shanmugam, S.; Cuthbert, J.; Flum, J.; Fantin, M.; Boyer, C.; Kowalewski, T.; Matyjaszewski, K., Transformation of gels via catalyst-free selective RAFT photoactivation. *Polymer Chemistry* **2019,** *10* (19), 2477-2483.

21. Bagheri, A.; Engel, K. E.; Bainbridge, C. W. A.; Xu, J.; Boyer, C.; Jin, J., 3D printing of polymeric materials based on photo-RAFT polymerization. *Polymer Chemistry* **2020,** *11* (3), 641-647.

22. Bagheri, A.; Bainbridge, C. W. A.; Engel, K. E.; Qiao, G. G.; Xu, J.; Boyer, C.; Jin, J., Oxygen Tolerant PET-RAFT Facilitated 3D Printing of Polymeric Materials under Visible LEDs. *ACS Applied Polymer Materials* **2020,** *2* (2), 782-790.

23. Fu, Q.; Xie, K.; McKenzie, T. G.; Qiao, G. G., Trithiocarbonates as intrinsic photoredox catalysts and RAFT agents for oxygen tolerant controlled radical polymerization. *Polymer Chemistry* **2017,** *8* (9), 1519-1526.

24. Wu, C.; Corrigan, N.; Lim, C.-H.; Jung, K.; Zhu, J.; Miyake, G.; Xu, J.; Boyer, C., Guiding the design of organic photocatalyst for PET-RAFT polymerization: Halogenated xanthene dyes. *Macromolecules* **2018,** *52* (1), 236-248.

25. Nomeir, B.; Fabre, O.; Ferji, K., Effect of Tertiary Amines on the Photoinduced Electron Transfer-Reversible Addition–Fragmentation Chain Transfer (PET-RAFT) Polymerization. *Macromolecules* **2019,** *52* (18), 6898-6903.

26. Krause, S.; Gormley, J. J.; Roman, N.; Shetter, J. A.; Watanabe, W. H., Glass temperatures of some acrylic polymers. *Journal of Polymer Science Part A: General Papers* **1965,** *3* (10), 3573-3586.

27. Ju, H.; McCloskey, B. D.; Sagle, A. C.; Kusuma, V. A.; Freeman, B. D., Preparation and characterization of crosslinked poly (ethylene glycol) diacrylate hydrogels as fouling-resistant membrane coating materials. *Journal of Membrane Science* **2009,** *330* (1-2), 180-188.

28. Shanmugam, S.; Xu, S.; Adnan, N. N. M.; Boyer, C., Heterogeneous photocatalysis as a means for improving recyclability of organocatalyst in “Living” radical polymerization. *Macromolecules* **2018,** *51* (3), 779-790.

29. Zivic, N.; Bouzrati-Zerelli, M.; Kermagoret, A.; Dumur, F.; Fouassier, J. P.; Gigmes, D.; Lalevee, J., Photocatalysts in polymerization reactions. *ChemCatChem* **2016,** *8* (9), 1617-1631.

30. Herculano, L. S.; Malacarne, L. C.; Zanuto, V. S.; Lukasievicz, G. V. B.; Capeloto, O. A.; Astrath, N. G. C., Investigation of the photobleaching process of eosin Y in aqueous solution by thermal lens spectroscopy. *The Journal of Physical Chemistry B* **2013,** *117* (6), 1932-1937.

31. Song, L.; Varma, C. A.; Verhoeven, J. W.; Tanke, H. J., Influence of the triplet excited state on the photobleaching kinetics of fluorescein in microscopy. *Biophysical journal* **1996,** *70* (6), 2959.

32. Flory, P. J., *Principles of polymer chemistry*. Cornell University Press: 1953.

33. Fox Jr, T. G.; Flory, P. J. J. J. o. A. P., Second-order transition temperatures and related properties of polystyrene. I. Influence of molecular weight. **1950,** *21* (6), 581-591.

34. Stockmayer, W. H. J. T. J. o. c. p., Theory of molecular size distribution and gel formation in branched-chain polymers. **1943,** *11* (2), 45-55.

35. Grinberg, D.; Siddique, S.; Le, M. Q.; Liang, R.; Capsal, J. F.; Cottinet, P. J., 4D Printing based piezoelectric composite for medical applications. *Journal of Polymer Science Part B: Polymer Physics* **2019,** *57* (2), 109-115.

36. Fernandes, C.; Heggannavar, G. B.; Kariduraganavar, M. Y.; Mitchell, G. R.; Alves, N.; Morouço, P. In *Smart Materials for Biomedical Applications: The Usefulness of Shape-Memory Polymers*, 2019; Trans Tech Publ: pp 237-247.

37. Kanu, N. J.; Gupta, E.; Vates, U. K.; Singh, G. K., An insight into biomimetic 4D printing. *RSC Advances* **2019,** *9* (65), 38209-38226.

38. Ge, L.; Dong, L.; Wang, D.; Ge, Q.; Gu, G., A digital light processing 3D printer for fast and high-precision fabrication of soft pneumatic actuators. *Sensors and Actuators A: Physical* **2018,** *273*, 285-292.

39. Agarwala, S.; Goh, G. L.; Goh, G. D.; Dikshit, V.; Yeong, W. Y., 3D and 4D printing of polymer/CNTs-based conductive composites. In *3D and 4D Printing of Polymer Nanocomposite Materials*, Elsevier: 2020; pp 297-324.

40. Zolfagharian, A.; Denk, M.; Bodaghi, M.; Kouzani, A. Z.; Kaynak, A., Topology-optimized 4D printing of a soft actuator. *Acta Mechanica Solida Sinica* **2019**, 1-13.

41. Yap, H. K.; Ng, H. Y.; Yeow, C.-H., High-force soft printable pneumatics for soft robotic applications. *Soft Robotics* **2016,** *3* (3), 144-158.

42. Tibbits, S., 4D printing: multi-material shape change. *Architectural Design* **2014,** *84* (1), 116-121.

43. Tibbits, S.; McKnelly, C.; Olguin, C.; Dikovsky, D.; Hirsch, S., 4D Printing and universal transformation. **2014**.

44. Gladman, A. S.; Matsumoto, E. A.; Nuzzo, R. G.; Mahadevan, L.; Lewis, J. A., Biomimetic 4D printing. *Nature materials* **2016,** *15* (4), 413-418.

45. Raviv, D.; Zhao, W.; McKnelly, C.; Papadopoulou, A.; Kadambi, A.; Shi, B.; Hirsch, S.; Dikovsky, D.; Zyracki, M.; Olguin, C., Active printed materials for complex self-evolving deformations. *Scientific reports* **2014,** *4*, 7422.

46. Ge, Q.; Qi, H. J.; Dunn, M. L., Active materials by four-dimension printing. *Applied Physics Letters* **2013,** *103* (13), 131901.

47. Ge, Q.; Dunn, C. K.; Qi, H. J.; Dunn, M. L., Active origami by 4D printing. *Smart Materials and Structures* **2014,** *23* (9), 094007.

48. Mao, Y.; Yu, K.; Isakov, M. S.; Wu, J.; Dunn, M. L.; Qi, H. J., Sequential self-folding structures by 3D printed digital shape memory polymers. *Scientific reports* **2015,** *5*, 13616.

49. Yu, K.; Dunn, M. L.; Qi, H. J., Digital manufacture of shape changing components. *Extreme Mechanics Letters* **2015,** *4*, 9-17.

50. Wu, J.; Yuan, C.; Ding, Z.; Isakov, M.; Mao, Y.; Wang, T.; Dunn, M. L.; Qi, H. J., Multi-shape active composites by 3D printing of digital shape memory polymers. *Scientific reports* **2016,** *6*, 24224.

51. Coulter, F. B.; Ianakiev, A., 4D printing inflatable silicone structures. *3D Printing and Additive Manufacturing* **2015,** *2* (3), 140-144.

52. Van Damme, J.; van den Berg, O.; Vlaminck, L.; Brancart, J.; Van Assche, G.; Du Prez, F., Anthracene-based polyurethane networks: Tunable thermal degradation, photochemical cure and stress-relaxation. *European Polymer Journal* **2018,** *105*, 412-420.

53. van der Schaaf, P. A.; Hafner, A.; Mühlebach, A., Photoinduced Ring-Opening Metathesis Polymerization (PROMP) with Photochemically Generated Schrock-Type Catalysts. *Angewandte Chemie International Edition in English* **1996,** *35* (16), 1845-1847.

54. Chung, C.-M.; Roh, Y.-S.; Cho, S.-Y.; Kim, J.-G., Crack healing in polymeric materials via photochemical [2+ 2] cycloaddition. *Chemistry of Materials* **2004,** *16* (21), 3982-3984.

55. Nojoomi, A.; Arslan, H.; Lee, K.; Yum, K., Bioinspired 3D structures with programmable morphologies and motions. *Nature Communications* **2018,** *9* (1), 3705.

56. Ryu, J.; D'Amato, M.; Cui, X.; Long, K. N.; Jerry Qi, H.; Dunn, M. L., Photo-origami—Bending and folding polymers with light. *Applied Physics Letters* **2012,** *100* (16), 161908.

57. Mu, X.; Sowan, N.; Tumbic, J. A.; Bowman, C. N.; Mather, P. T.; Qi, H. J., Photo-induced bending in a light-activated polymer laminated composite. *Soft Matter* **2015,** *11* (13), 2673-2682.

58. Li, M.; Fromel, M.; Ranaweera, D.; Rocha, S.; Boyer, C.; Pester, C. W., SI-PET-RAFT: Surface-Initiated Photoinduced Electron Transfer-Reversible Addition–Fragmentation Chain Transfer Polymerization. *ACS Macro Letters* **2019,** *8* (4), 374-380.